HAL open science

Electrochemical investigations of Nb2O5/carbon materials from filter paper, microfibrillated and bacterial celluloses by sustainable reductive mineralization

Aurélien Henry, Steven Le Vot, Johan Alauzun, Peter Hesemann, Maria Foresti, Patricia Cerruti, Laurent Heux, Olivier Fontaine, Bruno Boury

To cite this version:

Aurélien Henry, Steven Le Vot, Johan Alauzun, Peter Hesemann, Maria Foresti, et al.. Electrochemical investigations of Nb2O5/carbon materials from filter paper, microfibrillated and bacterial celluloses by sustainable reductive mineralization. Electrochimica Acta, 2019, 313, pp.478-487. 10.1016/j.electacta.2019.04.077 . hal-02169361

HAL Id: hal-02169361

https://hal.umontpellier.fr/hal-02169361v1

Submitted on 22 Oct 2021

HAL is a multi-disciplinary open access archive for the deposit and dissemination of scientific research documents, whether they are published or not. The documents may come from teaching and research institutions in France or abroad, or from public or private research centers.

L'archive ouverte pluridisciplinaire **HAL**, est destinée au dépôt et à la diffusion de documents scientifiques de niveau recherche, publiés ou non, émanant des établissements d'enseignement et de recherche français ou étrangers, des laboratoires publics ou privés.

Distributed under a Creative Commons Attribution - NonCommercial 4.0 International License

Version of Record: https://www.sciencedirect.com/science/article/pii/S0013468619307637
Manuscript_a2c862bae2efe1803ae4ccadbc15d6e7

Electrochemical investigations of Nb_2O_5/carbon materials from filter paper, microfibrillated and bacterial celluloses by sustainable reductive mineralization.

Aurélien Henry,[a] Steven Le Vot,[a,d] Johan G. Alauzun,[a] Peter Hesemann,[a] Maria L. Foresti,[b] Patricia Cerruti,[b] Laurent Heux,[c] Olivier Fontaine,[a,d]* Bruno Boury[a]*

[a] Institut Charles Gerhardt de Montpellier, UMR 5253, Université de Montpellier, CNRS, ENSCM, 34095 Montpellier Cedex 5, France

[b] Instituto de Tecnología en Polímeros y Nanotecnología (ITPN), Facultad de Ingeniería, Universidad de Buenos Aires, CONICET Las Heras 2214, CP 1127AAR Buenos Aires, Argentina

[c] CERMAV-CNRS, 601 rue de la Chimie, St Martin d'Hères 38041 Grenoble Cedex 9 (France)

[d] Réseau sur le Stockage Electrochimique de l'Energie (RS2E), FR CNRS 3459, France

Abstract:

Cellulose is an attractive reagent for the elaboration of C-containing materials, but here, we also considered it as an O-provider for preparing macro, micro and nano-fibrous Nb_2O_5/C composites by a new mineralization with Nb_2Cl_{10} in anhydrous conditions. Our study highlights differences of reactivity between filter paper, microfibrillated or bacterial cellulose in connection with the crystallinity and the accessibility of the hydroxyl groups. The Nb_2O_5/C ratio was found to be adjustable (55-75% of Nb oxide) depending on the cellulosic precursor. Our composites were tested as electrodes that could be used as negative electrode in hybrid lithium-capacitor. Electrochemical characterizations of Nb_2O_5/C composites are reported and it was demonstrated that characteristics of the starting cellulosic reagents that influence physico-chemical properties of composites thus impact electrodes performances. Very interestingly, for 1C charging/discharging rates, capacities as good as thus of literature (150 mAh g^{-1}) were obtained using our new sustainable synthesis protocol.

Introduction

Electrode materials, used in energy storage devices such as batteries and supercapacitors, must now be designed at the nanoscale using green chemistry processes as much as possible [1] . Recently, semiconductor oxides like Nb_2O_5 and its composites that could be used for electrochemical applications, but also in catalysis, photocatalysis, field emission, photovoltaic, photodetector, sensor and as electrochromic material, attracted many interest [2-4]. Looking at electrochemical energy storage, Bard et

© 2019 published by Elsevier. This manuscript is made available under the CC BY NC user license
https://creativecommons.org/licenses/by-nc/4.0/

al. first demonstrated that Nb_2O_5 exhibits lithium and proton insertion [5, 6]. Compare to other possible materials for negative electrodes in hybrid-capacitors, Nb_2O_5 has a high theoretical capacity of ~200 mA h g^{-1} (*i.e.* higher than $Li_4Ti_5O_{12}$ and TiO_2, ~170 mA h g^{-1}) which would be effective for improving the energy density. Moreover, unlike commercial Li-ion-capacitors made using graphite, Nb_2O_5-based electrodes work in a voltage range free of potential safety problems associated with electrolyte decomposition, resulting in a stable and very long cycle life. Finally, prelithiation of negative electrode materials, which could be necessary to reach high energy density with fair cycling performance, are not required for Nb_2O_5-based electrodes [7-10].

For Nb_2O_5, the electrochemical performance is closely related to its crystal structure, which can be amorphous, pseudohexagonal (TT-), orthorhombic (T-), tetragonal (M-) or monoclinic (H-). Briefly, Nb_2O_5 orthorhombic (T- Nb_2O_5) crystalline phase have been shown to perform better than pseudohexagonal (TT- Nb_2O_5) or amorphous phase [7, 9, 11]. The excellent capacity and rate performance of nanostructured T-Nb_2O_5 have been attributed to the easy Li insertion along favoured crystallographic pathways and open channels of interconnected NbO_x sheets, leading to reduced energy barriers and improved local charge transfer in the structures [7-9, 12, 13].

The morphology, at the nanoscale, is the second key criterion according to Dunn *et al*. [8, 9]. Like for other metal oxides, carbon has been assembled with niobium pentoxide with two aims. The first aim is to improve the poor electrical conductivity of Nb_2O_5 ($\pm$ 3 10^{-6} S cm^{-1}). This can be done by combining Nb_2O_5 nanoparticles with conductive scaffolds of carbon nanotubes [14-16], graphene [17], reduced graphene oxide [18], or carbide-derived carbon [19, 20]. Secondly, the sintering of Nb_2O_5 nanoparticles is detrimental because of specific surface area decreasing which can occur during the thermal treatment that is necessary for T-Nb_2O_5 formation (> 600°C). To prevent this, a Ta-substitution was proposed in the literature to achieve stabilized Nb_2O_5 polymorph [21]. However, wrapping nanoparticles with carbon coatings appears to be the easiest way to prevent this phenomenon.

Different approaches have been investigated to do this, such as polymer templated sol-gel processing of niobium oxide precursors in which the polymer (Igepal CO-520 [22], PEO-*b*-PS[23-26], is converted into carbon upon pyrolysis. In hydrothermal processes, resorcinol/formaldehyde [17, 27], sucrose [28] and glucose [29], have been used as a water soluble source of carbon. Insoluble cellulose [30-32] or cellulose acetate [33, 34] were the first sacrificial templates used to control Nb_2O_5 particle growth. In terms of fibers, pure Nb_2O_5 polymorphe and Nb_2O_5/C composite have been prepared respectively by electrospinning of sol-gel solution mixed with polyvinylpyrrolidone as carrier [35, 36] or electrospinning of powder of Nb_2O_5 mixed with polyvinylalcohols as carrier [37]. Recently, graphene

[38], reduced graphene oxide [39, 40] or carbon microspheres [27] were used to synthesize Nb2O5/C composites but these approaches suffer from lack of scalability. On the other hand, cellulose has recently been the focus of renewed attention and, for example, insoluble nanocrystals were used as a template for the development of Nb_2O_5 composites prepared by a sol-gel route but in that case reactivity of cellulose was not engaged and even was not used a carbon-phase precursor [41].

Using a very innovative method, our approach to use cellulose for processing such metal oxides and metal oxide/carbon composites is very different. Recently we reported a new approach to limit solvent and reagent use, to work at low temperature while using the cheapest and greenest reagents. Completely differently from all the other previous work using cellulose, here, cellulose provides the oxygen required for metal oxide formation, and serves also as a carbon precursor for the metal oxide/carbon composite [42-45]. This allows to avoid any sol-gel process using solvent and solution chemistry. By this inexpensive, simple and as sustainable as possible process, we reported the mineralization of cellulose to obtain highly anisotropic morphologies like nanoplates, needles and flowers. Their formation is apparently linked to the reactivity of cellulose and similar morphology has never been reported when cellulose is combined with the sol-gel route to metal oxides. Moreover, for example, in the case of TiO_2/C, a deposit of a few nanometers of carbon on metal oxide nanoparticles was evidenced. These data prompted us to consider that this process could be a possible route to obtain new efficient Nb_2O_5/carbon nanocomposites.

Thus, we report in this article the first study that highlights the possibility offered by cellulose for preparing metal oxide and metal oxide/carbon composite investigating Nb_2O_5 as the metal oxide due to its attractive properties, especially for electrochemical applications. Nb_2O_5/C nanocomposites were prepared using new route that we have developed, and the effect of the cellulose morphology crystallinity and size were studied. We found that Nb_2O_5/C nanocomposites prepared using micro-fibrillated cellulose (MFC) allowed preparing electrodes with capacity of more than 150 mAh g^{-1} at 1C that exhibits same performances than the literature but prepared with much more complex procedures.

Experimental

Materials. Diniobium(V) decachloride (Nb_2Cl_{10}) and dichloromethane (CH_2Cl_2) are of analytical grade from Across (France). Dichloromethane was freshly distilled over P_2O_5 before used. Filter paper FP-3-101-090 is from Sartorius (France). Aerogel of micro-fibrillated cellulose (MFC) was prepared by freeze-drying from *t*-butanol solvent exchanged suspensions according to the procedure previously described [46]. Aerogel of bacterial cellulose (BC) were prepared according to a previously reported procedure then

freeze dried from water solution [47]. All cellulosic materials were dried 3 days in an oven at 80°C just before use. All manipulations with Nb_2Cl_{10} and dried nanocellulose aerogel were performed in a glove box under argon atmosphere (<10 ppm of water).

Instrumentation. The X-ray powder diffraction (XRPD) patterns of the samples were recorded using a diffractometer (Philips X'Pert Pro, Netherlands). Raman spectra were obtained using Horiba LabRAM ARAMIS, Japan, with excitation wavelength of 633 nm. FT-IR were recorded on crushed powders with a Spectrum 2 (PerkinElmer) in ATR mode after accumulation of 16 scans. N_2-physisorption isotherms were obtained at 77 K using Micromeritics Tristar, USA. The samples were outgassed for 12 h at 150°C under vacuum (2 Pa). The pore size distribution was calculated from the desorption branch using the BJH method. Thermogravimetric analyses (TGA) were obtained using Netzsch Simultaneous Thermal Analyser STA 409 PC Luxx and Setaram Labsys TGA-DSC. Scanning electronic microscopy (SEM) images were obtained with a Hitachi S-4800, Canada. Energy dispersive X-ray analysis (EDAX) was done using the EDAX attachment (Oxford Instruments, UK) of the SEM system.

Preparation of NbO_x@FP, NbO_x@BC and NbO_x@MFC. In a glove box under inert atmosphere (< 2 ppm H_2O), cellulose source (FP, MFC or BC), dichloromethane (30 mL), and Niobium(V) pentachloride were placed into a Teflon-lined autoclave (in quantities described in table S1), and placed in an oven at 85°C for 3 days. When cooled down to room temperature, black residue was washed with anhydrous dichloromethane (3 x 20 mL). Then, under ambient atmosphere, residues were subsequently washed with standard dichloromethane (3 x 20 mL), and dried in an oven at 80°C for 24 h. Sample obtained are named: NbO_x@FP, NbO_x@BC and NbO_x@MFC, respectively according to cellulosic precursor used.

Thermal treatments. Pyrolysis under argon was performed at 800 °C, for 1 h, at a heating rate of 5°C min^{-1}, yielding the corresponding samples called Nb_2O_5-C^{FP}, Nb_2O_5-C^{BC}, Nb_2O_5-C^{MFC}, respectively.

Electrochemical characterizations. All electrochemical characterizations were performed in Swagelok® cell at room temperature on an MPG2 instrument from BioLogic by using Teflon-made Swagelok® cell. All electrodes were composed of the active material, acetylene black (as conductive additive) and carboxymethylcellulose (as binder) according to the following mass ratio: 80:8:12. After stirring in water, the mixture was spread uniformly onto a copper current collector using a 3540 bird film applicator from Elecometer leading to electrode thickness of about 150 µm. Lithium metal disks were used as both reference and counter electrodes, and Whatman glass fibers filters were used as separator. The electrolyte was 1 M $LiPF_6$ in a 1:1:3 solution of ethylene carbonate, propylene carbonate and dimethylcarbonate. All electrochemical results are provided taking into account the mass of the active material, *i.e.* the mass of

the Nb_2O_5/C composite. For galvanostatic measurements, the cells were charged and discharged at various C rates from 1 C to 1000 C (1 C corresponding to 100 mA g^{-1}). For cyclic voltammetry, all cells were cycled at various scan rates ranging from 0.5 to 500 mV s^{-1}.

Results and discussion

In order to synthesize Nb_2O_5/C electrodes, the strategy that was chosen include a first mineralization step of the cellulosic precursor by Nb_2Cl_{10}, in anhydrous conditions followed by a calcination step to obtain the desired crystalline phase for the niobium dioxide.

Mineralization of Cellulosic support by Nb_2Cl_{10} in anhydrous conditions. A first interesting result is that, when mineralization was performed at 85°C, the recovered hybrid materials, either NbO_x@FP, NbO_x@BC and NbO_x@MFC present shape and mechanical consistency with the starting cellulosic material, except the final colour that was black, and this whatever the type of cellulose used (Figure. S1). XRD experiments show that although they are broadened, similar signals than cellulose precursor, are observed in the corresponding hybrid samples before any thermal treatment (Figure. 1). Consequently, at 85°C, the crystal structure of cellulose is partially preserved. At that stage of the synthesis process, no niobium-containing inorganic crystalline phase could be identified. Materials from this mineralization process was actually deeply characterized and FTIR and Raman analyses can be find in supplementary information (Figures. S2 and S3). ^{13}C SS NMR was used to determine the crystallinity of samples and spectra are shown in figure 2. For all the samples, the spectra displayed features typical of native cellulose that have been already abundantly described in the literature in terms of allomorphic ratio and crystallinity. Bacterial cellulose BC sample exhibits mainly Iα phase and a high degree of crystallinity, whereas FP and MFC are predominantly Iβ, with intermediate and lower crystallinity, respectively. An interesting conclusion is that the reaction seems to have partially preserved the integrity of the crystalline organization of the initial substrate, known to be sensitive to thermal or chemical transformation. Degree of crystallinity of the samples was determined by integrating the C4 signals from the crystalline (between 86 and 92 ppm) and the disordered contributions (between 80 and 86 ppm). The results give crystallinity indices of 0.57 for MFC, 0.65 for FP and 0.82 for BC. This is in good agreement with the fact that the elementary nanocrystals are smaller in MFC, of intermediate size for FP and even bigger in BC, so that the surface to volume ratio is lower for bacterial cellulose. For~~,~~ composites, NbOx@FP, NbOx@MCF, NbOx@BC, integrations of these contributions represent~~s~~ a molar fraction of 0.11, 0.08 and less than 0.02 for MFC, FP and BC respectively. This is in good agreement with the results obtained on the crystalline and disordered contributions, showing that the consumption of cellulose is directly

proportional to the amount of hydroxyl exposed at the surface, and hence on the crystallinity of the sample.

The second step of the process is to calcinate the NbO_x@FP, NbO_x@BC and NbO_x@MFC to obtain the desired Nb_2O_5/C composites. X-ray diffraction experiments as a function of the temperature was performed between ambient temperature and 1100°C and it was conclude that a heating to 800°C correspond to the optimal condition to obtain T-Nb_2O_5 without large crystallites. Indeed this structure is believed to be the most efficient considering the application of Nb_2O_5 as material for electrochemical energy storage device) [7]. More details about these XRD experiments are available in supplementary information (Figure. S4 and table S2). In order to improve clarity of the discussion that follows, only samples prepared at 800°C are going to be considered in this manuscript.

Structural characterization Nb_2O_5-C^{FP}, Nb_2O_5-C^{BC} and Nb_2O_5-C^{MFC}. At first, morphological and chemical characterizations were performed by SEM, TEM and EDX. SEM images (Figure. 3) show a good preservation of the fibrous structure of the starting cellulosic support (Figure. S5) and Nb_2O_5 particles are visible at the surface of the carbon left by the carbonization. For sample Nb_2O_5-C^{BC} and Nb_2O_5-C^{MFC}, the assembly of Nb_2O_5 nanocrystals and carbonaceous network is homogeneous at the nanoscale. For sample prepared with FP, the situation is less homogeneous, big pieces of carbonaceous residue being mixed with micro and sub-micrometer particles of niobium oxide. An EDX mapping of the elements confirms a complete and homogenous covering of C, O and Nb for all the samples, and an example is given for Nb_2O_5-C^{BC} in figure S5. Figure 4 shows HRETM images for the most performant material (see below) Nb_2O_5-C^{MFC} to better understand its nanostructure. At the lowest magnification, a micro- to nano-fibrillated structure is observed in good agreement with MEB analyses. Some separated aggregates of inorganic nanoparticles are present but the major part of the material is made of nanoparticles of Nb_2O_5 (20-50 nm) well dispersed along the carbonaceous fibrils (Figure 4B, C and D). This is confirmed by EDX analysis showing that, spotting on large zone (> 100 nm) evidences the presence of C, Nb and O (Figure S6). At higher magnifications, in small dark low-density zones (< 20 nm) only C is detectable along with O, although with much lower intensity for this latter. At the opposite, high-density zones exhibit high intensity for rays of Nb and O, however, C rays is also clearly present although in lower intensity. This is in agreement with the images that reveals a highly disordered and poorly graphitized carbon layer of few nanometres thickness ≈1-5 nm covering the Nb_2O_5 nanoparticles (Figure 4B, C, D and E).

A very important thing to evaluate the performance of the electrodes is to know the Nb2O5/C weight ratio. To do this, TGA analyses in air and in argon were performed and show weight losses starting in all

cases around ≈100°C, much lower than the one of the pristine celluloses (180-200°C) (Figure. S6). This is ascribed to elimination of adsorbed volatile compound and elimination of HCl arising from condensation/hydrolysis of residual Nb-Cl and Nb-OH (from mineralization). In air, elimination of the carbonaceous residue by combustion is complete by 450°C; yields are reported in table 1. Under argon, the weight loss due to carbonization of the cellulosic residue occurs up to 1000°C, although it results to higher yields. Combining these TGA yields under air and argon and assuming that carbon results from the carbonization of cellulose, allows estimating the Nb_2O_5/C mass ratio of the different samples and they are summarized in table 1. Comparison of the samples shows that the proportion of carbon is the highest for samples prepared with FP (~45%) and the lowest is for samples prepared from MFC (~25%), the one for sample prepared from BC being in between around 30%. Interestingly this process give access to a proportion of carbon that is in-between the lowest one obtained with surfactant (Igepal® CO520 7% of C [22] and PEO-PS 11% of C) [23], and the highest obtained with saccharides and resins (sucrose 59-87% of C [28] and resorcinol-formaldehyde:70-75% of C[17]). The resulting amounts of carbon for the three precursors used, are in line with the results shown by SS-NMR. Our findings show a lower production of NbO_x for the more crystalline substrate and higher rates for the less crystalline, and hence more reactive substrates exposing a higher number of hydroxyl groups. This is an important result because it could open new opportunities for the tailoring Nb_2O_5/C composites containing predictable amount of oxide, and hence a ratio of carbon/oxide that can be finely tuned.

XRD measurements after bulk pyrolysis (Figure. S7) allowed the determination of the crystallographic structure and the evaluation of the crystallite's size. Nb_2O_5-C^{FP} presents a mix of two phases: an orthorhombic T-Nb_2O_5 (ICSD 30-0873, 2θ =22.6, 28.4, 36.5, 46.1 and 55.2°) and a tetragonal NbO_2 (ICSD 76-0682, 2θ =26.0, 35.2, 37.1, 40.0 and 52.0°), no quantitative ratio is proposed due to overlapping of signals. The T-Nb_2O_5 phase seems to be the most present, even if it has smaller crystallites (30 nm) than the NbO_2 one (58 nm). Nb_2O_5-C^{MFC} presents also a mix of NbO_2 and Nb_2O_5, the latter being in major proportion. The crystallite sizes of the two phases are this time very close (25 and 24 nm, respectively).

Finally, it is necessary to know the surface area of our synthesized compounds as electrochemical surface area is directly related the performance of electrochemical devices. However, it is unfortunately a very difficult information to get, especially considering carbonaceous materials and oxides. Nevertheless, it is usual, and accepted, to consider the BET specific surface area to discuss morphological properties of the samples (porosity, external surface etc…). Nitrogen adsorption and desorption isotherms were recorded (Figure. S8) and BET surface area (total surface), the micrometric surface and the mesoporous surface

(also called external surface) were determined (Table 2). Composite obtained from FP and BC cellulose show similar characteristic with BET surface of about 200 m^2 g^{-1} including 50 m^2 g^{-1} of microporous area (25 %). Interestingly, MCF cellulosic reagent lead to the highest BET surface area (372 m^2 g^{-1}) with a microporous surface of 258 m^2 g^{-1} representing 70 % of the total surface. Specific surface area and especially pore size distribution are very important to keep in mind when looking at the electrochemical properties. Table 3 also summarize the total pore volume for the composites and the average pore size for samples obtained from three different cellulosic reagent.

Electrochemical evaluation of the Nb_2O_5/C composites. In this study, electrochemical characteristic of our Nb_2O_5/C composites were investigated using cyclic voltammetry and galvanostatic cycling and results are discussed in following paragraph. It is not the purpose of this study to claim that we present a real supercapacitors, but rather than we evaluate candidates that could be used as negative electrodes in an hybride Li-capacitor.

Cyclic voltammetry is a very convenient technic to study electrochemical behaviour of our composites. Figure 5a) shows the CVs for Nb_2O_5-C^{MFC} at the lowest scan rates. As, it is known, the peak current is related to the scan rate as expressed in the following equation (eq. 1) [7]:

$$i = av^b \qquad \text{(eq. 1)}$$

where i is the peak current (A), ν is the scan rate (mV s^{-1}) and a and b are adjustable variables. Particularly, the b-values gives precious information about electrochemical mechanism. A value of 0.5 indicates that process is purely diffusional whereas a value of 1 indicates a thin-film behaviour. A b-value between 0.5 and 1 would indicate a process that is governed by restricted diffusion [7]. Figure 6 shows the evolution of the current as a function a scan rate (logarithm scale). b-values can be extracted from the slopes that are observed. For our 3 cellulosic precursors, the general is the same. At lowest scan rates b is 0.7 for Nb_2O_5-C^{FP} and Nb_2O_5-C^{BC} and b equal 0.8 for Nb_2O_5-C^{MFC}. When scan rate becomes more important slope decreases, a b-value reaches 0.5 in every cases. Two-well defined area can be observed. In a first one, at lowest scan rates, the process is governed by a restricted diffusion whereas when scan rate increases, process is governed by semi-infinite linear diffusion.

On the other hand, for this kind of pseudo-capacitive materials, it is usual to discuss the relative contribution of surface capacitive current and diffusion-controlled intercalation process [48, 49]. At a fixed potential, the current response, that allows to distinguish the two mechanisms is expressed according the following relation (eq. 2):

$$i(V) = k_1 v + k_2 v^{0.5} \quad \text{(eq. 2)}$$

Where, $k_1 v$ is the current relative to surface capacitive effect and $k_2 v^{0.5}$ is the current relative to diffusion intercalation process. As explained in previous references, for analytical purpose the equation is rearrange and expressed as follows (eq. 3):

$$\frac{I(V)}{v^{0.5}} = k_1 v^{0.5} + k_2 \quad \text{(eq. 3)}$$

When I(V) $v^{-0.5}$ is plot as a function of the square root of the scan rate, k1 and k2 can be quantified, k_1 being the slope of the curve and k_2 the y-axis intercept.

For all our device, independently of the type of cellulosic precursor used to synthesized the Nb_2O_5 / C composite, this separation between the two above-mentioned mechanisms was, in fact, impossible. This indicates that our materials never behave according to one or the other type mechanism. To prove this, the normalized current I $v^{-0.5}$ was plot as a function of the potential (figure 5b). If process were governed by diffusion-controlled intercalation process, curves for different scan rates should overlap, at least at one potential. This is obviously not the case and this comfort the current peak analysis (figure 6) that showed that our process is a governed by restricted diffusion on the whole potential range and never exclusively governed by one of the particular case described above. However, and because it is an important point to discuss, capacitive contribution of the electrode, which can be attributed to carbon from the composite, have been estimated by integration of the area define by the lower and upper potential of the positive scan and the value of pure capacitive current determined at high potential versus Li^+/Li (around 2.7 – 2.8 V). For all CVs presented in figure 5a, capacitive contribution was found to be close to 20%. It is important to mention that this value, although low, is likely over estimated because, according to literature [48, 49] the capacitive contribution in the faradaic region should be lower than this taken into account to determine this value of 20%. Actually, even if carbon contribution cannot be considered as negligible, this proves that the storage performance of our electrode comes mostly from the Nb_2O_5 pseudocapacitive material.

More than any, what is important in this study is the comparison and the discussion about the three new sustainable synthesis methods that allowed preparing Nb_2O_5/carbon composites. Cyclic voltammograms for the three different kinds of Nb_2O_5-C (from 3 different cellulose), are shown in figure 7. Both anodic and cathodic peaks are broad, but they flatten down as the sweep rate decreases. This is an expected

behaviour for these kind of intercalation materials. The comparison of the three samples shows an important difference between the specific currents measured on the different materials. Nb_2O_5-C^{MFC} presents higher specific currents than the two other. This is consistent with physico-chemical characterisations which showed that synthesis with MCF cellulose leads to higher specific area, nicely dispersed Nb2O5 particles, highest N_2O_5 / C ratio etc… It is important to notice that the poorest sample in terms of carbon ratio exhibits the best electrochemical performance versus lithium intercalation, proving that carbon contribution to the specific capacitance is almost insignificant compare to Nb_2O_5 contribution. Moreover, fact that carbon does not explain capacitance values can be seen on CVs between 2.5 and 3.0 V vs. Li^+/Li where the "capacitive area" related to ion adsorption on carbon surface is very low compare to the niobium region between 1.2 and 2.5 V vs. Li^+/Li.

Another feature that have to be highlighted is that, if the peak shift is continuous for Nb_2O_5-C^{MFC}, it can be noticed that, for the two other samples, the voltammogramms with a sweep rate higher than 200 mV s^{-1} are almost stackable, with a disappearance of the two peaks. It suggests that, for Nb2O5-C^{BC} and Nb_2O_5-C^{FP}, beyond 200 mV s^{-1}, the sweep rate is too fast for exchanging Li^+ between the electrodes on the investigated potential window. These results highlight that different cellulosic precursors lead to different electrochemical behaviour and thus that performances of Nb_2O_5 could be further optimized if a more suitable precursors were used.

Galvanostatic cyclings at different charging / discharging rates were performed on each sample and voltage profiles are presented in figure 8. 10 cycles were recorded for each rate and are all shown. As we can see, the ten cycles are almost stackable, which is very interesting particularly at high charging/discharging rates. This indicate a good stability even under fast solicitation. After 20 cycles, each electrode reaches a coulombic efficiency higher than 99 %. Similarly, to the cyclic voltammetry, an important difference of performances can be observed between Nb_2O_5-C^{MFC} and the two other samples. At c-rate of 1C, Nb_2O_5-C^{MFC} presents a reversible capacity of ~ 150 mAh g^{-1}, whereas Nb_2O_5-C^{FP} and Nb_2O_5-C^{BC} ones are only close to 70 mAh g^{-1}. Another important feature is that the galvanostatic curves do not present any insertion plateau, which is characteristic of nanosized insertion materials and of a pseudo-capacitive behavior. In such systems, the specific area of the material is expected to have a great influence on electrochemical performances.

The specific capacity provided by Nb_2O_5-C^{FP}, Nb_2O_5-C^{BC} and Nb_2O_5-C^{MFC} according to the C-rate (where C is set at 100.8 mA g^{-1} for one electron process) is presented in figure 8. Usually C-rate is a common metric for battery materials and not for supercapacitors. However, we decided to use it in order to match the data from Dunn et al publication which is the reference for Nb_2O_5 [7]. For a better clarity,

each dot represents the capacity of the tenth discharge for the considered C-rate. As a comparison, values from Augustyn et al. (a) [7], Zhang et al. (b) [50] and Kong et al. (c) [41] are also given. For low C-rate capacity is as good as this of the reference publications indicating that our sustainable synthesis is very promising for pseudo-capacitor materials. The following decrease of the capacity of our materials is more pronounced than those of Dunn et al., what could be attributed to the presence of the less favourable NbO_2 phase in our samples. Further development on cellulosic precursors will permit to accommodate this issue. Once again, another notable feature is the difference of capacity between Nb_2O_5-C^{MFC} and the two other samples. This difference is consistent to the gap of specific area between the samples. indeed, for a charging/discharging rate of 1C, our best material, Nb_2O_5-C^{MFC}800, exhibits a capacity of ~150 mAh g^{-1} and it have a specific area of 370 m^2 g^{-1}, compare with the ~70 mAh g^{-1} and 200 m^2 g^{-1} for Nb_2O_5-C^{BC}, the two samples having similar Nb_2O_5/C ratios (respectively 75 and 70 wt.% of Nb_2O_5). On the other hand, the capacity of Nb_2O_5-C^{FP} is ~67 mAh g^{-1}, and can be attributed to the combination of a lower content in Nb_2O_5 (55 wt.%) and a higher specific area (245 m^2 g^{-1}) than Nb_2O_5-C^{BC}. These results demonstrate unambiguously that our three composites possess the same intrinsic storage performances. However, as a very interesting finding, the Nb_2O_5-C^{MFC} synthesis allowed to double the electrochemical surface of Nb_2O_5-C materials and thus to double their capacity.

A very important thing that has to be noticed is that we did not performed prolonged cycling, at least in classic way, because we assume that our composites are still not optimized and it wouldn't be relevant to start time-consuming experiments in these conditions. However, figure 9 shows the evolution of the capacity as a function of the C-rate. For each charging / discharging rate, 10 galvanostatic cycles were recorded. As expected, capacity, decreases when solicitation becomes more important (time for charge and discharge becomes shorter). Actually, the very interesting thing is that after the solicitation at 1000C, when a charging / discharging C-rate of 1C is applied once again, the initial capacity is reached. The device has not only been cycled 180 times, (from 1C – to 1000C) but also with high solicitations (as high as 1000C). This clearly highlights that our materials can be cycles more than 200 hundreds times and at high charging/discharging rate without any loss of capacity.

These findings are very important because they open many opportunities to design new efficient Nb_2O_5/C composites to be used in hybrid supercapacitors from cheap precursors and using a sustainable process.

Conclusions

The above set of results shows a new aspect of the reactivity of cellulose, the latter being directly dehydrated with the cheapest and greenest niobium reagent, niobium(V) chloride, at low temperature. Therefore, the resulting Nb_2O_5/C composites can be prepared by a simple and up-scalable protocol. It is highlighted that all the cellulosic fibers are not equivalent, indeed comparison of filter paper, bacterial cellulose and microfibrillated cellulose shows that the latter is the best for elaborating a homogeneous and performant nanocomposite, thanks to its low crystallinity, small size and, consequently, the low proportion of carbon that is left after pyrolysis. In relation with that, electrochemical properties, toward Li-intercalation, are in the range of those reported in literature to date and that prepared by much more sophisticated and expensive methods like hydrothermal or polymer templated approach. It is very encouraging to consider our synthesis as a new efficient way to prepare Nb_2O_5/C composites that could be tested as real negative electrode in a hybrid Li-capacitor. Considering that cellulose precursor allow tuning crystallographic structure, BET surface, microporosity, oxide/carbon ratio, morphologie of oxide particles etc… our results highlight the benefit of our approach to develop new enhanced architecture for energy storage applications from natural polysaccharides.

Conflicts of interest

There are no conflicts to declare

Acknowledgements

Mr Cot is warmly acknowledged for SEM analyses at IEMM.

Notes and references

[1] A.S. Arico, P. Bruce, B. Scrosati, J.-M. Tarascon, W. van Schalkwijk, Nanostructured materials for advanced energy conversion and storage devices, Nat Mater, 4 (2005) 366-377.
[2] R.S. Devan, R.A. Patil, J.-H. Lin, Y.-R. Ma, One-Dimensional Metal-Oxide Nanostructures: Recent Developments in Synthesis, Characterization, and Applications, Advanced Functional Materials, 22 (2012) 3326-3370.
[3] R.A. Rani, A.S. Zoolfakar, A.P. O'Mullane, M.W. Austin, K. Kalantar-Zadeh, Thin films and nanostructures of niobium pentoxide: fundamental properties, synthesis methods and applications, Journal of Materials Chemistry A, 2 (2014) 15683-15703.
[4] J. Zhao, Y. Gu, J. Huang, Flame synthesis of hierarchical nanotubular rutile titania derived from natural cellulose substance, Chemical communications, 47 (2011) 10551-10553.
[5] B. Reichman, A.J. Bard, Electrochromism at Niobium Pentoxide Electrodes in Aqueous and Acetonitrile Solutions, Journal of The Electrochemical Society, 127 (1980) 241-242.
[6] B. Reichman, A.J. Bard, The Application of Nb2O5 as a Cathode in Nonaqueous Lithium Cells, Journal of The Electrochemical Society, 128 (1981) 344-346.

[7] V. Augustyn, J. Come, M.A. Lowe, J.W. Kim, P.-L. Taberna, S.H. Tolbert, H.D. Abruña, P. Simon, B. Dunn, High-rate electrochemical energy storage through Li+ intercalation pseudocapacitance, Nat Mater, 12 (2013) 518-522.
[8] J. Come, V. Augustyn, J.W. Kim, P. Rozier, P.-L. Taberna, P. Gogotsi, J.W. Long, B. Dunn, P. Simon, Electrochemical Kinetics of Nanostructured Nb2O5 Electrodes, Journal of The Electrochemical Society, 161 (2014) A718-A725.
[9] J.W. Kim, V. Augustyn, B. Dunn, The Effect of Crystallinity on the Rapid Pseudocapacitive Response of Nb2O5, Advanced Energy Materials, 2 (2012) 141-148.
[10] K. Naoi, S. Ishimoto, J.-i. Miyamoto, W. Naoi, Second generation 'nanohybrid supercapacitor': Evolution of capacitive energy storage devices, Energy & Environmental Science, 5 (2012) 9363-9373.
[11] B. Orel, M. Maček, J. Grdadolnik, A. Meden, In situ UV-Vis and ex situ IR spectroelectrochemical investigations of amorphous and crystalline electrochromic Nb2O5 films in charged/discharged states, Journal of Solid State Electrochemistry, 2 (1998) 221-236.
[12] A.A. Lubimtsev, P.R.C. Kent, B.G. Sumpter, P. Ganesh, Understanding the origin of high-rate intercalation pseudocapacitance in Nb2O5 crystals, Journal of Materials Chemistry A, 1 (2013) 14951-14956.
[13] R. Kodama, Y. Terada, I. Nakai, S. Komaba, N. Kumagai, Electrochemical and In Situ XAFS-XRD Investigation of Nb2O5 for Rechargeable Lithium Batteries, Journal of The Electrochemical Society, 153 (2006) A583-A588.
[14] G. Luo, H. Li, D. Zhang, L. Gao, T. Lin, A template-free synthesis via alkaline route for Nb2O5/carbon nanotubes composite as pseudo-capacitor material with high-rate performance, Electrochimica Acta, 235 (2017) 175-181.
[15] X. Wang, G. Li, Z. Chen, V. Augustyn, X. Ma, G. Wang, B. Dunn, Y. Lu, High-Performance Supercapacitors Based on Nanocomposites of Nb2O5 Nanocrystals and Carbon Nanotubes, Advanced Energy Materials, 1 (2011) 1089-1093.
[16] X. Wang, G. Li, R. Tjandra, X. Fan, X. Xiao, A. Yu, Fast lithium-ion storage of Nb2O5 nanocrystals in situ grown on carbon nanotubes for high-performance asymmetric supercapacitors, RSC Advances, 5 (2015) 41179-41185.
[17] L. Kong, X. Cao, J. Wang, W. Qiao, L. Ling, D. Long, Revisiting Li+ intercalation into various crystalline phases of Nb2O5 anchored on graphene sheets as pseudocapacitive electrodes, Journal of Power Sources, 309 (2016) 42-49.
[18] E. Lim, C. Jo, M.S. Kim, M.-H. Kim, J. Chun, H. Kim, J. Park, K.C. Roh, K. Kang, S. Yoon, J. Lee, High-Performance Sodium-Ion Hybrid Supercapacitor Based on Nb2O5@Carbon Core–Shell Nanoparticles and Reduced Graphene Oxide Nanocomposites, Advanced Functional Materials, 26 (2016) 3711-3719.
[19] C. Zhang, M. Beidaghi, M. Naguib, M.R. Lukatskaya, M.-Q. Zhao, B. Dyatkin, K.M. Cook, S.J. Kim, B. Eng, X. Xiao, D. Long, W. Qiao, B. Dunn, Y. Gogotsi, Synthesis and Charge Storage Properties of Hierarchical Niobium Pentoxide/Carbon/Niobium Carbide (MXene) Hybrid Materials, Chemistry of Materials, 28 (2016) 3937-3943.
[20] C. Zhang, R. Maloney, M.R. Lukatskaya, M. Beidaghi, B. Dyatkin, E. Perre, D. Long, W. Qiao, B. Dunn, Y. Gogotsi, Synthesis and electrochemical properties of niobium pentoxide deposited on layered carbide-derived carbon, Journal of Power Sources, 274 (2015) 121-129.
[21] A. Le Viet, M.V. Reddy, R. Jose, B.V.R. Chowdari, S. Ramakrishna, Electrochemical properties of bare and Ta-substituted Nb2O5 nanostructures, Electrochimica Acta, 56 (2011) 1518-1528.
[22] S.Y. Lim, W. Shen, Z. Gao, Carbon quantum dots and their applications, Chemical Society Reviews, 44 (2015) 362-381.
[23] E. Lim, H. Kim, C. Jo, J. Chun, K. Ku, S. Kim, H.I. Lee, I.-S. Nam, S. Yoon, K. Kang, J. Lee, Advanced Hybrid Supercapacitor Based on a Mesoporous Niobium Pentoxide/Carbon as High-Performance Anode, ACS nano, 8 (2014) 8968-8978.

[24] H. Kim, E. Lim, C. Jo, G. Yoon, J. Hwang, S. Jeong, J. Lee, K. Kang, Ordered-mesoporous Nb2O5/carbon composite as a sodium insertion material, Nano Energy, 16 (2015) 62-70.
[25] I.E. Rauda, V. Augustyn, B. Dunn, S.H. Tolbert, Enhancing Pseudocapacitive Charge Storage in Polymer Templated Mesoporous Materials, Accounts of Chemical Research, 46 (2013) 1113-1124.
[26] J. Lee, M. Christopher Orilall, S.C. Warren, M. Kamperman, F.J. DiSalvo, U. Wiesner, Direct access to thermally stable and highly crystalline mesoporous transition-metal oxides with uniform pores, Nature Materials, 7 (2008) 222.
[27] L. Kong, C. Zhang, J. Wang, W. Qiao, L. Ling, D. Long, Nanoarchitectured Nb2O5 hollow, Nb2O5@carbon and NbO2@carbon Core-Shell Microspheres for Ultrahigh-Rate Intercalation Pseudocapacitors, Scientific reports, 6 (2016) 21177.
[28] G. Li, X. Wang, X. Ma, Nb2O5-carbon core-shell nanocomposite as anode material for lithium ion battery, Journal of Energy Chemistry, 22 (2013) 357-362.
[29] H. Xiong, H.N. Pham, A.K. Datye, A facile approach for the synthesis of niobia/carbon composites having improved hydrothermal stability for aqueous-phase reactions, Journal of Catalysis, 302 (2013) 93-100.
[30] L.J. Maschio, P.H.F. Pereira, M.L.C.P. da Silva, Preparation and characterization of cellulose/hydrous niobium oxide hybrid, Carbohydrate Polymers, 89 (2012) 992-996.
[31] F.A. Pavan, M.S.P. Francisco, R. Landers, Y. Gushikem, Adsorption of phosphoric acid on niobium oxide coated cellulose fiber: preparation, characterization and ion exchange property, Journal of the Brazilian Chemical Society, 16 (2005) 815-820.
[32] E.A. Campos, Y. Gushikem, M. do Carmo Gonçalves, S.C. de Castro, Preparation and Characterization of Niobium Oxide Coated Cellulose Fiber, Journal of Colloid and Interface Science, 180 (1996) 453-459.
[33] E.A. Campos, Y. Gushikem, Composite Membrane of Niobium(V) Oxide and Cellulose Acetate: Preparation and Characterization, Journal of Colloid and Interface Science, 193 (1997) 121-126.
[34] A.G.S. Prado, E.A. Faria, J.R. SouzaDe, J.D. Torres, Ammonium complex of niobium as a precursor for the hydrothermal preparation of cellulose acetate/Nb2O5 photocatalyst, Journal of Molecular Catalysis A: Chemical, 237 (2005) 115-119.
[35] A.L. Viet, M.V. Reddy, R. Jose, B.V.R. Chowdari, S. Ramakrishna, Nanostructured Nb2O5 Polymorphs by Electrospinning for Rechargeable Lithium Batteries, The Journal of Physical Chemistry C, 114 (2010) 664-671.
[36] A. Tolosa, B. Krüner, S. Fleischmann, N. Jäckel, M. Zeiger, M. Aslan, I. Grobelsek, V. Presser, Niobium carbide nanofibers as a versatile precursor for high power supercapacitor and high energy battery electrodes, Journal of Materials Chemistry A, 4 (2016) 16003-16016.
[37] K. Nakane, M. Morinaga, N. Ogata, Formation of niobium oxide and carbide nanofibers from poly(vinyl alcohol)/niobium oxide composite nanofibers, Journal of Materials Science, 48 (2013) 7774-7779.
[38] Q. Deng, M. Li, J. Wang, K. Jiang, Z. Hu, J. Chu, Free-anchored Nb2O5@graphene networks for ultrafast-stable lithium storage, Nanotechnology, 29 (2018) 185401.
[39] Y. Jiao, H. Zhang, H. Zhang, A. Liu, Y. Liu, S. Zhang, Highly bonded T-Nb2O5/rGO nanohybrids for 4 V quasi-solid state asymmetric supercapacitors with improved electrochemical performance, Nano Research, 11 (2018) 4673-4685.
[40] S. Li, T. Wang, W. Zhu, J. Lian, Y. Huang, Y.-Y. Yu, J. Qiu, Y. Zhao, Y.-C. Yong, H. Li, Controllable synthesis of uniform mesoporous H-Nb2O5/rGO nanocomposites for advanced lithium ion hybrid supercapacitors, Journal of Materials Chemistry A, 7 (2019) 693-703.
[41] L. Kong, C. Zhang, J. Wang, D. Long, W. Qiao, L. Ling, Ultrahigh intercalation pseudocapacitance of mesoporous orthorhombic niobium pentoxide from a novel cellulose nanocrystal template, Materials Chemistry and Physics, 149-150 (2015) 495-504.

[42] A. Henry, N. Louvain, O. Fontaine, L. Stievano, L. Monconduit, B. Boury, Synthesis of Titania@Carbon Nanocomposite from Urea-Impregnated Cellulose for Efficient Lithium and Sodium Batteries, ChemSusChem, 9 (2016) 264-273.
[43] A. Henry, S. Plumejeau, L. Heux, N. Louvain, L. Monconduit, L. Stievano, B. Boury, Conversion of nanocellulose aerogel into TiO2 and TiO2@C nano-thorns by direct anhydrous mineralization with TiCl4. Evaluation of electrochemical properties in Li batteries, ACS Applied Materials and Interfaces, (2015).
[44] G.R. Nair, S.K. Samdarshi, B. Boury, Surface Mineralization of Cellulose by Metal Chloride – an Original Pathway for the Synthesis of Hierarchical Urchin and Needle Carpetlike TiO2 Superstructures, European Journal of Inorganic Chemistry, 2013 (2013) 5303-5310.
[45] S. Plumejeau, M. Rivallin, S. Brosillon, A. Ayral, B. Boury, M-Doped TiO2 and TiO2–MxOy Mixed Oxides (M = V, Bi, W) by Reactive Mineralization of Cellulose – Evaluation of Their Photocatalytic Activity, European Journal of Inorganic Chemistry, 2016 (2016) 1200-1205.
[46] M. Fumagalli, D. Ouhab, S. Molina-Boisseau, L. Heux, Versatile Gas-Phase Reactions for Surface to Bulk Esterification of Cellulose Microfibrils Aerogels, Biomacromolecules, (2013).
[47] P. Cerrutti, P. Roldán, R.M. García, M.A. Galvagno, A. Vázquez, M.L. Foresti, Production of bacterial nanocellulose from wine industry residues: Importance of fermentation time on pellicle characteristics, Journal of Applied Polymer Science, 133 (2016) 43109-43118.
[48] T. Brezesinski, J. Wang, J. Polleux, B. Dunn, S.H. Tolbert, Templated Nanocrystal-Based Porous TiO2 Films for Next-Generation Electrochemical Capacitors, Journal of the American Chemical Society, 131 (2009) 1802-1809.
[49] J. Wang, J. Polleux, J. Lim, B. Dunn, Pseudocapacitive Contributions to Electrochemical Energy Storage in TiO2 (Anatase) Nanoparticles, The Journal of Physical Chemistry C, 111 (2007) 14925-14931.
[50] N. Zhang, Z. Liu, T. Yang, C. Liao, Z. Wang, K. Sun, Facile preparation of nanocrystalline Li4Ti5O12 and its high electrochemical performance as anode material for lithium-ion batteries, Electrochemistry Communications, 13 (2011) 654-656.

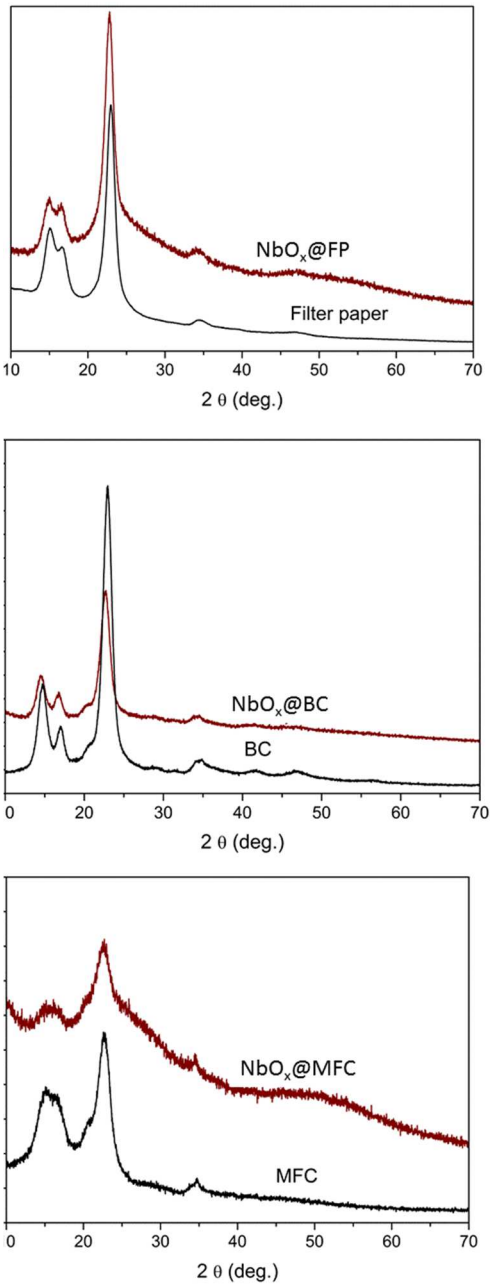

Fig. 1: X-ray diffraction patterns of cellulosic material (FP, MCF and BC) and the corresponding hybrid materials resulting from the mineralization process, respectively NbO_x@FP, NbO_x@MCF and NbO_x@BC.

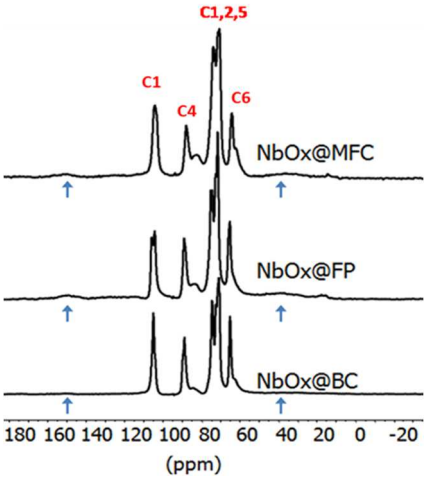

Fig. 2: ^{13}C SS NMR of hybrid materials resulting from the mineralization process respectively NbO_x@FP, NbO_x@MCF, NbO_x@BC.

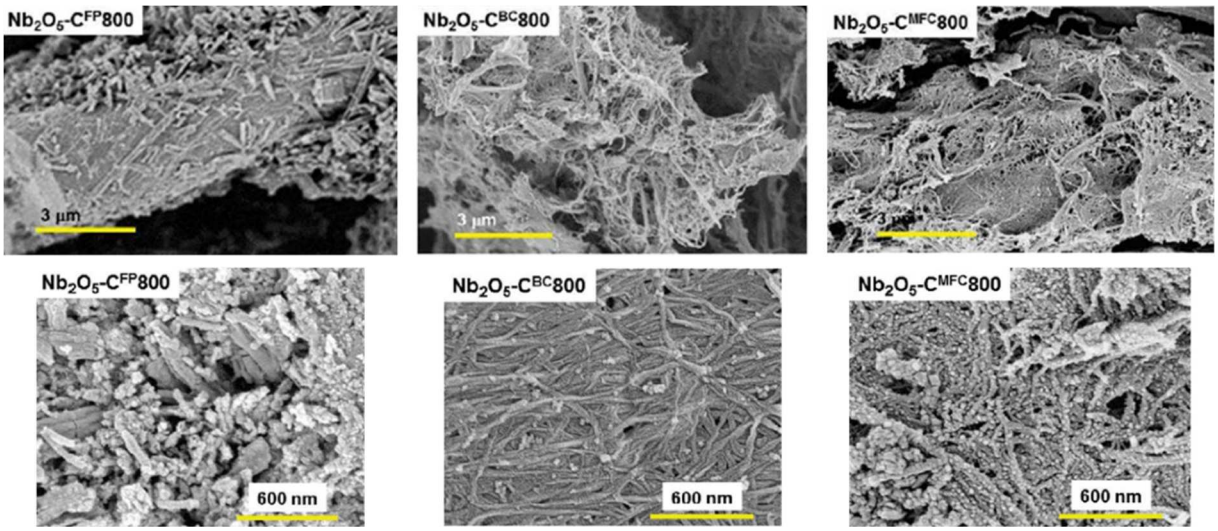

Fig. 3: SEM images magnifications of Nb_2O_5-C^{FP}800, Nb_2O_5-C^{BC}800 and Nb_2O_5-C^{MFC}800 resulting from the pyrolysis under argon of NbO_x@FP, NbO_x@MCF, NbO_x@BC.

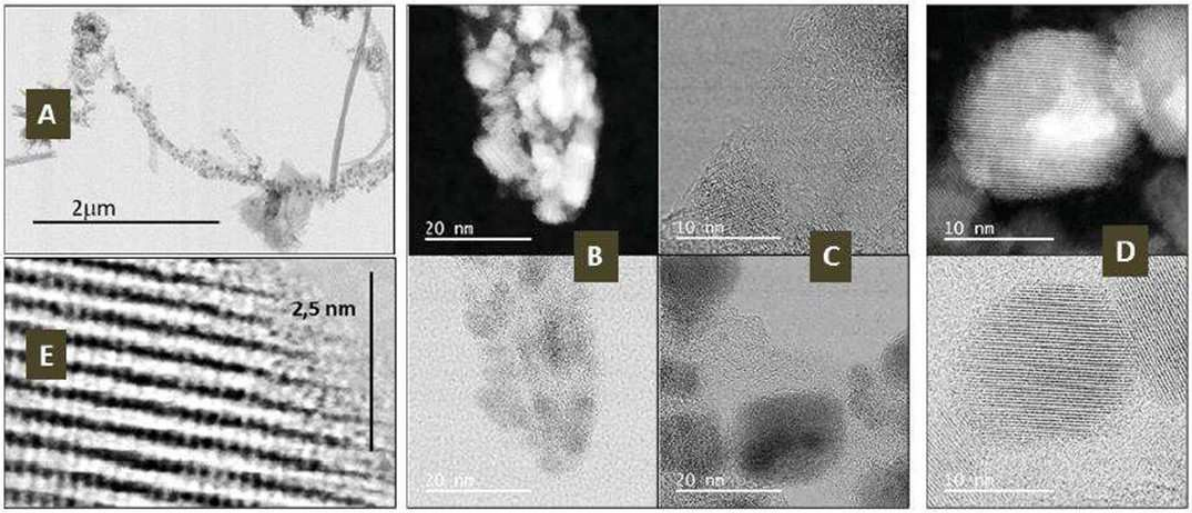

Fig. 4: HRTEM of Nb_2O_5-C^{MFC} resulting from the pyrolysis under argon of NbOx@MFC.

Starting sample	Name & Yield at 1000°C[a] Nb_2O_5	Name Yield at 800°C[b] Nb_2O_5/C (%)	Name Yield at 900°C[b] Nb_2O_5/C (%)
NbO_x@FP	$Nb_2O_5^{FP}$	$Nb_2O_5C^{FP}800$	$Nb_2O_5C^{FP}900$
	29.5 %	55,4%	54,3%
		53,1/46,7	54,3/45,6
NbO_x@BC	$Nb_2O_5^{BC}$	$Nb_2O_5C^{BC}800$	$Nb_2O_5C^{BC}900$
	19.5%	29,9%	27,1%
		65,2/34,8	72,0/28,0
NbO_x@MFC	$Nb_2O_5^{MCF}$	$Nb_2O_5C^{MFC}800$	$Nb_2O_5C^{MFC}900$
	35.0 %	48,3%	45,8%
		72,5/27,5	76,5/23,5

Table 1: Yields of TGA under air and argon of NbO_x@FP, NbO_x@BC and NbO_x@MFC, name of the corresponding sample after thermal treatment and Nb_2O_5/C composition. a: under air by TGA analysis; b: under argon and determined by TGA analysis.

Samples	S_{BET}[a]	S_{Micro}[b]	S_{Meso}	Vp[d]	Ø[e]
NbO_x@FP	48.9	4.2	44.7	0.18	99
NbO_x@BC	49.3	3.9	45.4	0.19	101
NbO_x@MFC	69.4	6.8	62.6	0.33	158
Nb_2O_5-C800^{FP}	192.6	49.5	143.1	0.36	65
Nb_2O_5-C800^{BC}	205.7	55.4	150.3	0.36	68
Nb_2O_5C800^{MFC}	372.3	258.5	113.8	0.39	75

Table 2: Summary of textural data obtained from N_2 porosimetry for sample before and after thermal treatment; [a]specific surface area (m^2 g^{-1}), [b]Total surface of micropores (m^2 g^{-1}) [c]Total surface of mesopores (m^2 g^{-1}) [d]total pore volume (cm^3 g^{-1}); [e]BJH average pore diameter calculated from the desorption branch (Å).

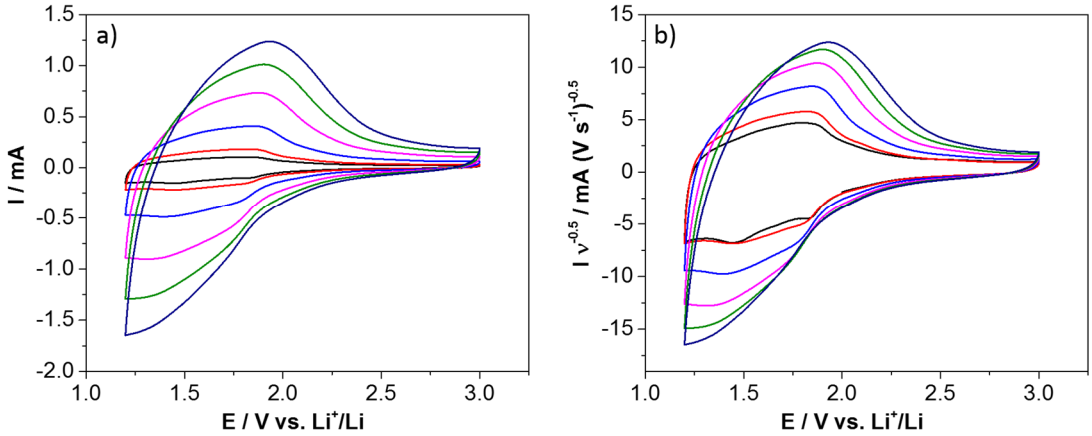

Fig. 5: a) Cyclic voltammogramms of Nb_2O_5-C^{MFC} at low scan rates (from 0.5 to 10 mV s^{-1}) and b) corresponding normalized CV (I $\nu^{-0.5}$ - E) to analyze electrochemical mechanisms.

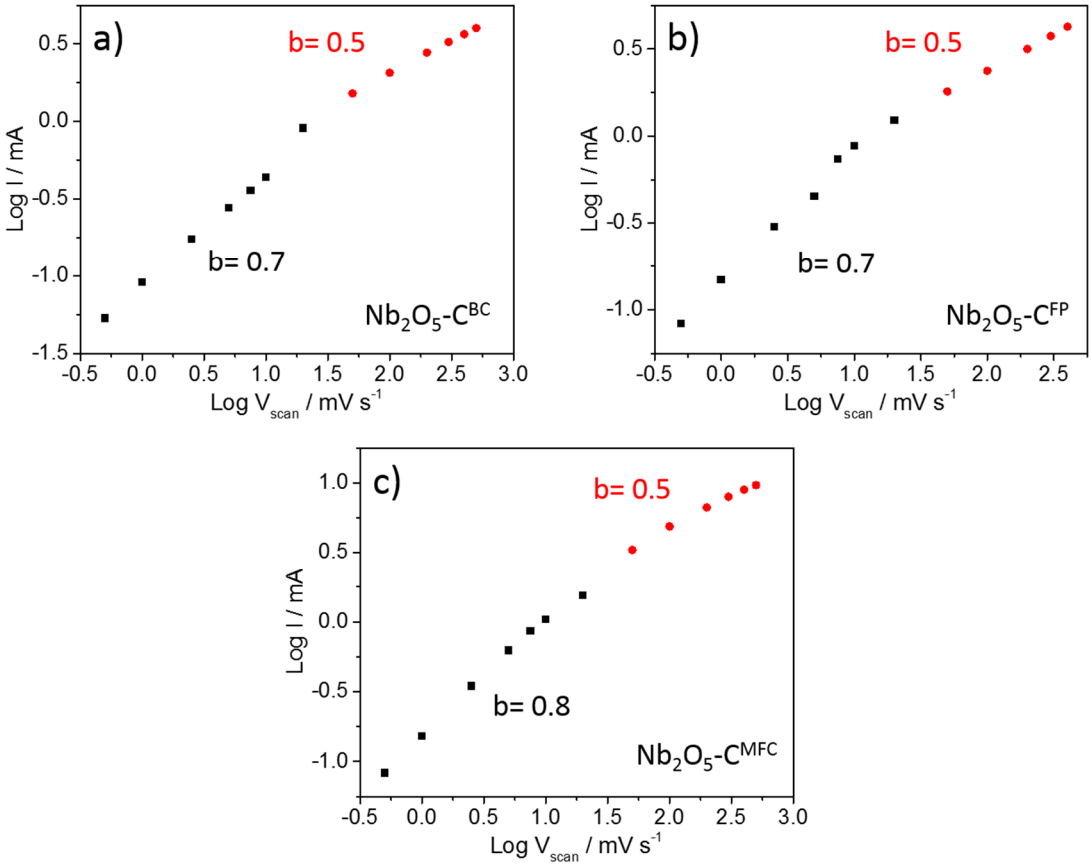

Fig. 6: Peak current analysis from CV of a) of Nb_2O_5-C^{BC}, a) of Nb_2O_5-C^{FP}, a) of Nb_2O_5-C^{MFC}

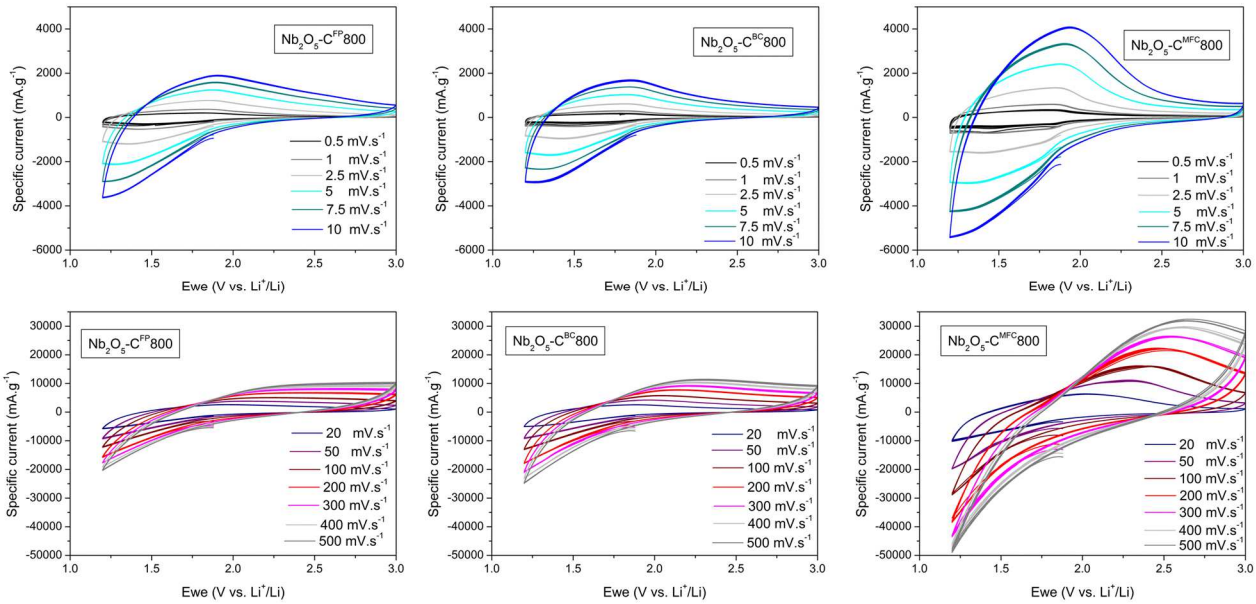

Fig. 7: Cyclic voltammogramms of a,b) Nb_2O_5-C^{MFC}800, c,d) Nb_2O_5-C^{BC}800 and e,f) Nb_2O_5-C^{FP}800.

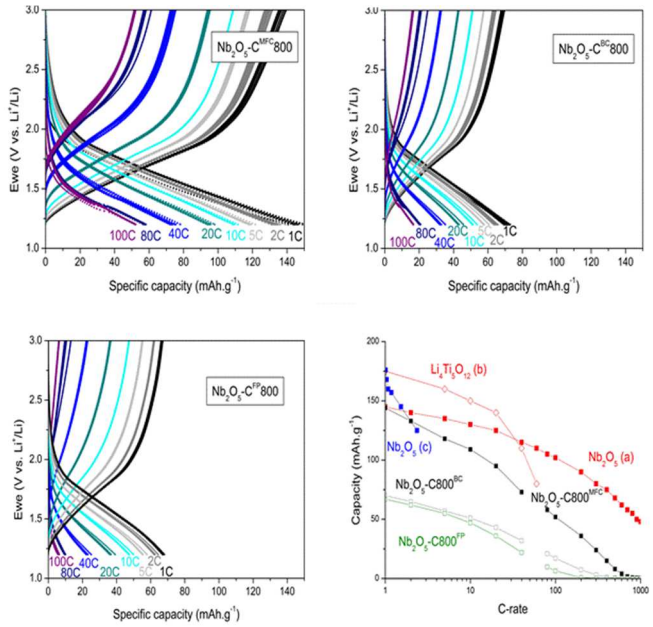

Fig. 8: C-rates of Nb_2O_5-C^{MFC}800, Nb_2O_5-C^{BC}800 and Nb_2O_5-C^{FP}800; comparison of the rate capacity of Nb_2O_5-C^{MFC}800, Nb_2O_5-C^{BC}800, Nb_2O_5-C^{FP}800 with *T*-Nb_2O_5, at various C-rates.

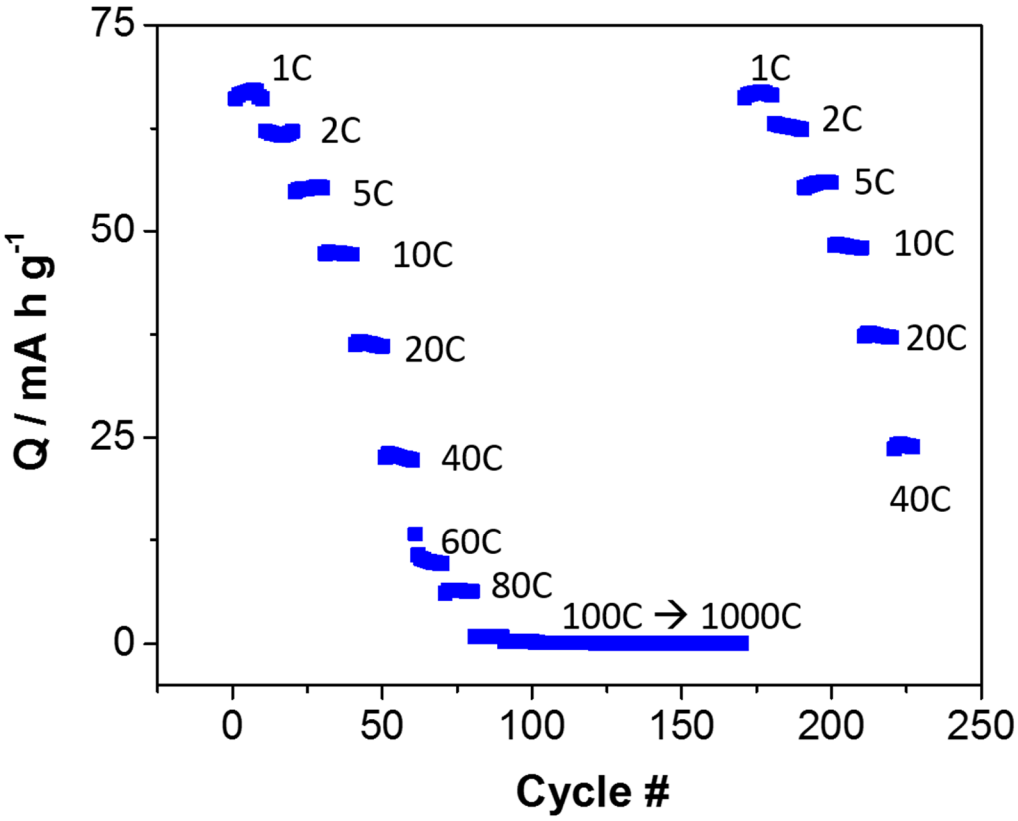

Fig. 9: Capacity of Nb_2O_5-C^{FP}800 as a function of cycle number and varying the C-rate.

Starting sample	Name & Yield at 1000°C[a] Nb_2O_5	Name Yield at 800°C[b] Nb_2O_5/C (%)	Name Yield at 900°C[b] Nb_2O_5/C (%)
NbO_x@FP	$Nb_2O_5^{FP}$	$Nb_2O_5C^{FP}800$	$Nb_2O_5C^{FP}900$
	29.5 %	55,4%	54,3%
		53,1/46,7	54,3/45,6
NbO_x@BC	$Nb_2O_5^{BC}$	$Nb_2O_5C^{BC}800$	$Nb_2O_5C^{BC}900$
	19.5%	29,9%	27,1%
		65,2/34,8	72,0/28,0
NbO_x@MFC	$Nb_2O_5^{MCF}$	$Nb_2O_5C^{MFC}800$	$Nb_2O_5C^{MFC}900$
	35.0 %	48,3%	45,8%
		72,5/27,5	76,5/23,5

Table 1: Yields of TGA under air and argon of NbO_x@FP, NbO_x@BC and NbO_x@MFC, name of the corresponding sample after thermal treatment and Nb_2O_5/C composition. a: under air by TGA analysis; b: under argon and determined by TGA analysis.

Samples	S_{BET}[a]	S_{Micro}[b]	S_{Meso}	Vp[d]	Ø[e]
NbO_x@FP	48.9	4.2	44.7	0.18	99
NbO_x@BC	49.3	3.9	45.4	0.19	101
NbO_x@MFC	69.4	6.8	62.6	0.33	158
Nb_2O_5-C800^{FP}	192.6	49.5	143.1	0.36	65
Nb_2O_5-C800^{BC}	205.7	55.4	150.3	0.36	68
Nb_2O_5C800^{MFC}	372.3	258.5	113.8	0.39	75

Table 2: Summary of textural data obtained from N_2 porosimetry for sample before and after thermal treatment; [a]specific surface area (m^2 g^{-1}), [b]Total surface of micropores (m^2 g^{-1}) [c]Total surface of mesopores (m^2 g^{-1}) [d]total pore volume (cm^3 g^{-1}); [e]BJH average pore diameter calculated from the desorption branch (Å).